

Transition to Chaos in the Self-Excited System with a Cubic Double Well Potential and Parametric Forcing

Grzegorz Litak,^{a,1} Marek Borowiec,^a Arkadiusz Syta,^b
Kazimierz Szabelski^a

^a*Department of Applied Mechanics, Technical University of Lublin, Nadbystrzycka 36, PL-20-618 Lublin, Poland*

^b*Department of Applied Mathematics, Technical University of Lublin, Nadbystrzycka 36, PL-20-618 Lublin, Poland*

Abstract

We examine the Melnikov criterion for a global homoclinic bifurcation and a possible transition to chaos in case of a single degree of freedom nonlinear oscillator with a symmetric double well nonlinear potential. The system was subjected simultaneously to parametric periodic forcing and self excitation via negative damping term. Detailed numerical studies confirm the analytical predictions and show that transitions from regular to chaotic types of motion are often associated with increasing the energy of an oscillator and its escape from a single well.

1 Introduction

A system of nonlinear stiffness having a square displacement force term, and simultaneously, excited externally or parametrically has been a subject of studies for many years [1,2,3,4,5,6,7,8,9,10]. It has found numerous applications in mechanical engineering [1,2,3,4,5,6,7,8] and control theory [9,10,11,12]. It was also one of intriguing examples of simple nonlinear systems which showed complex behaviour including chaotic oscillations [13]. Another important, partially separated, class of systems can be determined on the basis of nonlinear damping. Such damping can, in some systems, change the sign depending on velocity or displacement values, and provide excitation energy to the examined system. These, so called, self-excited damping terms are often used to describe

¹ Fax: +48-815250808; E-mail: g.litak@pollub.pl (G. Litak)

systems with dry friction, bearings lubricated by thin layer of oil, shimming in vehicle wheels or chatter in cutting process, [1,2,3,14,15]. More recently such a nonlinear damping force has also been considered [16] in modelling of a modern vehicle suspension system due to electro- or magneto-rheological fluid damping where it is causing a hysteretic effect. In this model [16] the authors used a self-excited term of Rayleigh type and Duffing double well potential.

This class of a system has also been investigated by Siewe *et al.* [17,18] in their works on Φ^6 -Van der Pol oscillators. In the first paper [17] they applied Melnikov approach and performed numerical simulations in case of a potential based on polynomials of even orders (4th and 6th orders: Φ^4 and Φ^6 type potentials respectively) and an external excitation. On the other hand in second paper [18] the triple well potential based on polynomial of the 6th order was studied in details for a dynamical system with external and parametric excitations. The Melnikov approach has been also considered in systems with a single well potential and various nonlinear damping terms. Among a large number of papers conducted that research we report [19,20,21]. Litak *et al.* [19] included the Rayleigh self-excited term to describe dynamics of the Froude pendulum, Trueba *et al.* [20] considered nonlinear damping following a power law in velocity ($\alpha(\dot{x})^n$, $n = 2, 3$) for various systems, and finally Awrejcewicz and Holicke [21] examined the effect of dry friction in a stick-slip system with the Duffing potential.

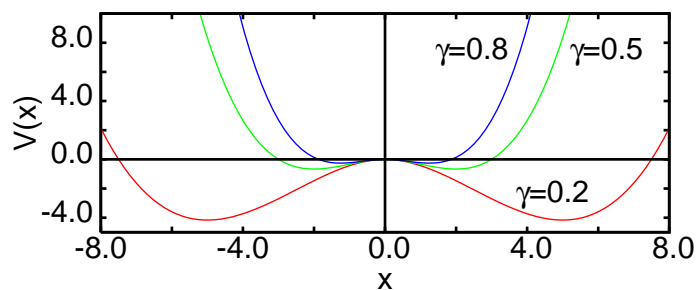


Fig. 1. The double well potential $V(x) = \delta x^2/2 + \gamma|x|x^2/3$ for three values of γ ($\gamma = 0.8, 0.5$, and 0.2) and $\delta = -1.0$.

Note, that all above systems can be still regarded as simple ones but its combined nonlinear answer on excitation is complicated and deserves detailed investigations.

In this note we shall examine transition from regular oscillations to chaos in a simple, one degree of freedom, system subjected to parametric and self excitations with a square albeit symmetric stiffness:

$$\ddot{x} + \alpha(-1 + x^2)\dot{x} + (\delta - \mu \cos 2\omega t)x + \gamma|x|x = 0, \quad (1)$$

where x is a displacement $\alpha(-1 + x^2)\dot{x}$ is nonlinear damping, $-\mu x \cos 2\omega t$ is

a parametric excitation while $\gamma|x|x$ and δx are square and linear force terms. It is worth mentioning that, the corresponding potential can be described by two polynomials of the 3rd order (Φ^3 type) for $x > 0$ and $x < 0$, respectively:

$$V(x) = \frac{\delta x^2}{2} + \frac{\gamma|x|x^2}{3} \quad (2)$$

and plotted in Fig. 1 for $\gamma = 0.2$, $\gamma = 0.5$ and $\gamma = 0.8$. In spite of appearing $|x|$ in Eq. 2 the function $V(x)$ is of C^2 class at $x = 0$ because it is approaching to 0, for $x \rightarrow 0$, as $\pm x^3$.

The present paper consists of three sections and two appendixes. After a short introduction in the present section (Sec. 1) we will examine the above system analytically and numerically in Sec. 2. There we will especially focus on a transition and a corresponding scenario from regular to chaotic vibrations. In Sec. 3 we will discuss the numerical simulations verifying the analytical findings. In the last section (Sec. 4) we will provide the summary and conclusions. In the appendixes we will present different treatment of a self-excitation term and its consequences to the applied analytical methods (Appendix A) and show the Melnikov integration procedures in details (Appendix B).

2 Melnikov Analysis

We are starting our study from the second order equation of motion (Eq. 1). After transforming it into two differential equations of the first order, a standard procedure in examining homoclinic transition will be applied to look for stable and unstable manifolds and their possible cross-sections in presence of weak excitations and damping. Therefore we have introduced a small parameter ε to the above equations enabling these terms to be switched on [4,22,23]:

$$\begin{aligned} \dot{x} &= v \\ \dot{v} &= -\delta x - \gamma|x|x + \varepsilon \left[\tilde{\alpha}(1 - x^2)v + x\tilde{\mu} \cos(2\omega t) \right], \end{aligned} \quad (3)$$

where $\tilde{\alpha}\varepsilon = \alpha$ and $\tilde{\mu}\varepsilon = \mu$. Note, that this is not a unique way of splitting the initial differential equation of the second order (Eq. 1) into two equations of the first order.

The other way is connected with different treatment of the self-excitation term. Basing on 'fast' and 'slow' variables (x, w) identification in Van der Pol fashion [24] we can write:

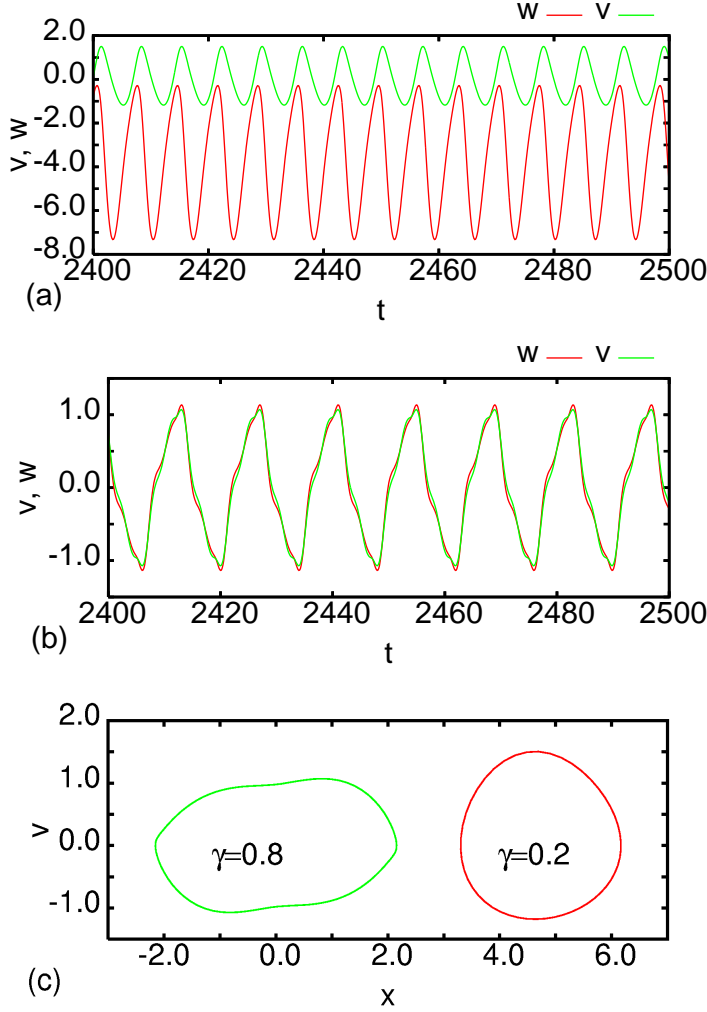


Fig. 2. Comparison of v and w time histories for $\gamma = 0.2$ (Fig. 2a) and $\gamma = 0.8$ (Fig. 2b). Other system parameters: $\alpha = 0.1$, $\omega = 0.45$, $\delta = -1.0$, $\mu = 0.6$. (Fig. 2c) Phase portraits (in $x-v$ space) of for both cases ($\gamma = 0.2$ and 0.8).

$$w = \dot{x} + \varepsilon \tilde{\alpha} \left(x - \frac{x^3}{3} \right). \quad (4)$$

This possibility has been examined thoroughly in Appendix A. Note, the difference between $w(t)$ and $v(t)$ depends on the influence of the self-excitation term leading to relaxation oscillations in the Van der Pol system. The time histories of w and v (Figs. 2a-b) show that this term could be more influential for smaller γ ($\gamma = 0.2$, Fig. 2a) while a case with larger γ ($\gamma = 0.8$, Fig. 1b) is apparently negligible. For better clarity we plotted phase portraits (Fig. 2c) for both cases showing that they correspond to steady state vibrations located in different regions of the phase plane. This is associated with differences in a potential shape (Fig. 1).

In the first case vibrations have been realized around the minimum of the

potential $V(x)$ ($x \approx 5.0$) inside one of its wells, while in the second one vibrations are located around $x = 0$ between $x = -2$ and 2 . As in the examined example the self-excitation Van der Pol term:

$$\text{VdP}(x, \dot{x}) = \alpha(-1 + x^2)\dot{x} \quad (5)$$

is changing its sign at $x = \pm 1.0$. One can easily see that for $\gamma = 0.2$ the system behaves if it possessed renormalised nonlinear damping term which does not change its sign. Moreover this term is positively defined. Thus the system, due to the shape of the external potential (Fig. 1), does not have any relaxation character typical for simple Van der Pol oscillator and the distinction of 'slow' and 'fast' variables is not relevant here. This fact has its reminiscence in a large difference in $v(t)$ and $w(t)$ time histories in Fig. 2a. The transformation $v(t) \rightarrow w(t)$ can be better argued in the the second examined case ($\gamma = 0.8$). There the relaxation vibrations are present but in this case the effect of self-excitation turns out be small (Fig. 2b).

Note, that the unperturbed Hamiltonian H^0 is the same for both cases (with v or w variables) and reads:

$$H^0 = \frac{v^2}{2} + V(x). \quad (6)$$

The potential function $V(x)$ (Fig. 1) has the local peak at $x_0 = 0$. The existence of this point with a horizontal tangent makes global homoclinic bifurcations, including transition from regular to chaotic solution, which may occur in the system. Obviously, at this point the system velocity reaches zero value ($v = 0$) (Fig. 1). Thus, according to our potential gauge, the total energy has only its potential part which is also zero:

$$E = V(x = 0) = 0. \quad (7)$$

Transforming Eqs. 4,6 for a constant energy, chosen here as zero, (Eq. 7) we obtain the following expression for velocity:

$$v = \frac{dx}{dt} = \sqrt{2 \left(-\frac{\delta x^2}{2} - \frac{\gamma |x|x^2}{3} \right)}, \quad (8)$$

from which

$$t - t_0 = \int \frac{1}{\sqrt{2 \left(-\frac{\delta x^2}{2} - \frac{\gamma |x|x^2}{3} \right)}} dx, \quad (9)$$

where t_0 represents an integration constant. As a result of integration (Eq. 9) we get so called homoclinic orbits (Fig. 3) parametrised by time t :

$$\begin{aligned} x^* &= x^*(t - t_0) = \pm \frac{3\delta}{2\gamma} \left(1 - \tanh^2 \left(\frac{\sqrt{-\delta}(t - t_0)}{2} \right) \right) \\ v^* &= v^*(t - t_0) = \mp \frac{3\delta\sqrt{-\delta}}{2\gamma} \frac{\tanh \left(\frac{\sqrt{-\delta}(t - t_0)}{2} \right)}{\cosh^2 \left(\frac{\sqrt{-\delta}(t - t_0)}{2} \right)}, \end{aligned} \quad (10)$$

where '+' and '-' signs are related to I and II orbits (Fig. 3), respectively.

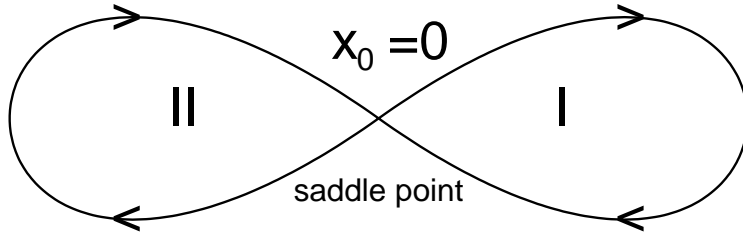


Fig. 3. Homoclinic orbits (I and II) of unperturbed potential $V(x) = -x^2/2 + |x|x^2/3$ (for $\delta = -1$ and $\gamma = 1$) in a phase plane (x, \dot{x}) . For $t \rightarrow \pm\infty$ we get $(x, \dot{x}) \rightarrow (x_0, \dot{x}_0) = (0, 0)$.

Note, the central saddle point $x_0 = 0$ is reached in time t corresponding to $+\infty$ and $-\infty$, respectively.

In case of perturbed orbits W^S (a stable manifold) and W^U (an unstable manifold) the distance between them is given by the Melnikov function $M(t_0)$ [22,23,26]:

$$M(t_0) = \int_{-\infty}^{+\infty} h(x^*, v^*) \wedge g(x^*, v^*) dt \quad (11)$$

where the corresponding differential forms h is the gradient of unperturbed Hamiltonian (Eq. 6):

$$h = (\delta x + \gamma|x^*|x^*) dx + v dv, \quad (12)$$

and g is a perturbation form (Eq. 3) to the same Hamiltonian (Eq. 6):

$$g = (\tilde{\mu}x \cos 2\omega\tau + \tilde{\alpha}(1 - x^2)v) dx \quad (13)$$

Both differential forms are defined on homoclinic manifold $(x, v) = (x^*, v^*)$ (Eq. 10, Fig. 2).

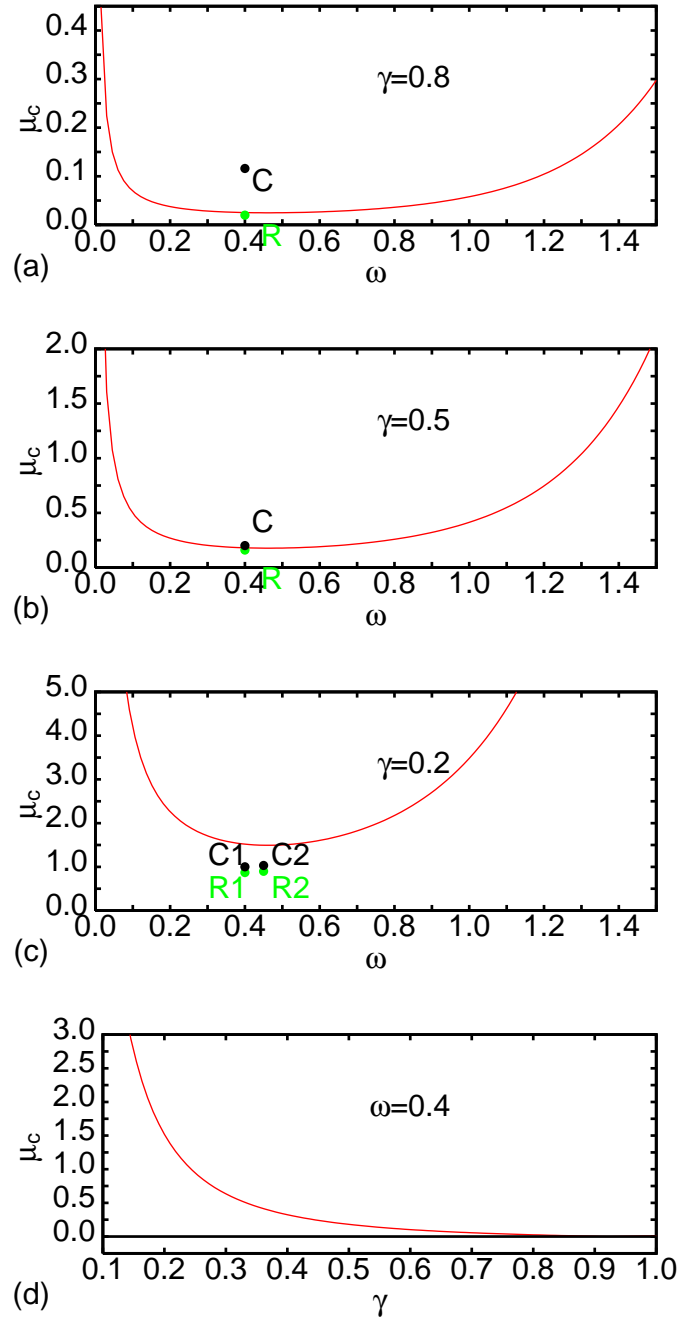


Fig. 4. Critical value of μ_c , for $\alpha = 0.1$, versus ω for $\delta = -1$ and various γ ($\gamma = 0.8$ (Fig. 4a), $\gamma = 0.5$ (Fig. 4b), $\gamma = 0.2$ (Fig. 4c)) and versus γ (Fig. 4d).

Naturally, from the above (Eqs. 11-13) the Melnikov integral is given by:

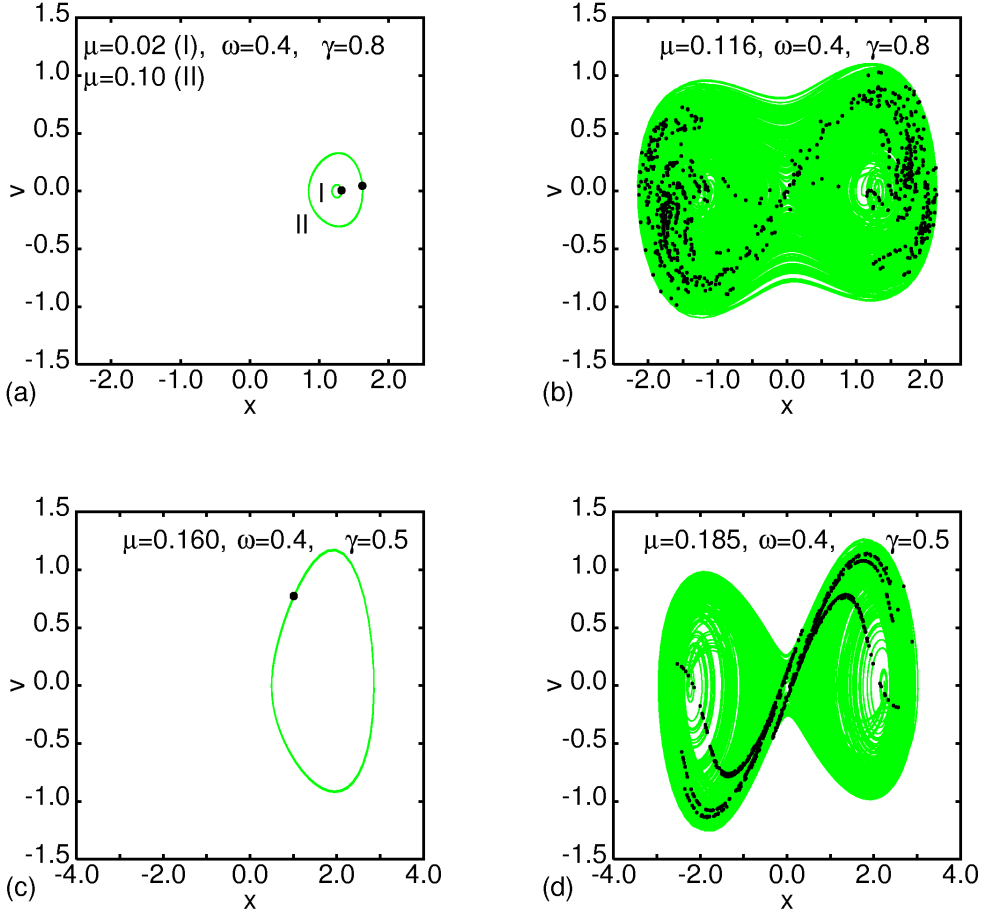


Fig. 5. Phase diagrams and Poincaré sections (simulations were based on Eq. 1) chosen sets system parameters $\alpha = 0.1$, $\delta = -1.0$ and μ , ω , γ (corresponding values are indicated in figures) denoted by points in Figs. 4a-d. The corresponding maximal Lyapunov exponent is (Fig. 5a): $\lambda_1 = -0.0279$ for '1' and $\lambda_1 = -0.0238$ for '2', (Fig. 5b): $\lambda_1 = 0.0903$, (Fig. 5c): $\lambda_1 = -0.0978$), (Fig. 5d): $\lambda_1 = 0.0812$, (Fig. 5e): $\lambda_1 = -0.1513$, (Fig. 5f): $\lambda_1 = 0.1202$, (Fig. 5g): $\lambda_1 = -0.1974$, (Fig. 5h): $\lambda_1 = 0.0529$, respectively.

$$\begin{aligned}
M(t_0) &= \int_{-\infty}^{+\infty} v^*(t-t_0) \left\{ \tilde{\mu} x^*(t-t_0) \cos(2\omega t) + \tilde{\alpha} [1-x^{*2}(t-t_0)] v^*(t-t_0) \right\} dt \\
&= \int_{-\infty}^{+\infty} v^*(t) \left\{ \tilde{\mu} x^*(t) \cos(2\omega(t+t_0)) + \tilde{\alpha} [1-x^{*2}(t)] v^*(t) \right\} dt. \quad (14)
\end{aligned}$$

After substituting $x^*(t)$ and $v^*(t)$ given in Eq. 10 we obtain:

$$M(t_0) = \tilde{\mu} I_1(t_0) + \tilde{\alpha} I_2, \quad (15)$$

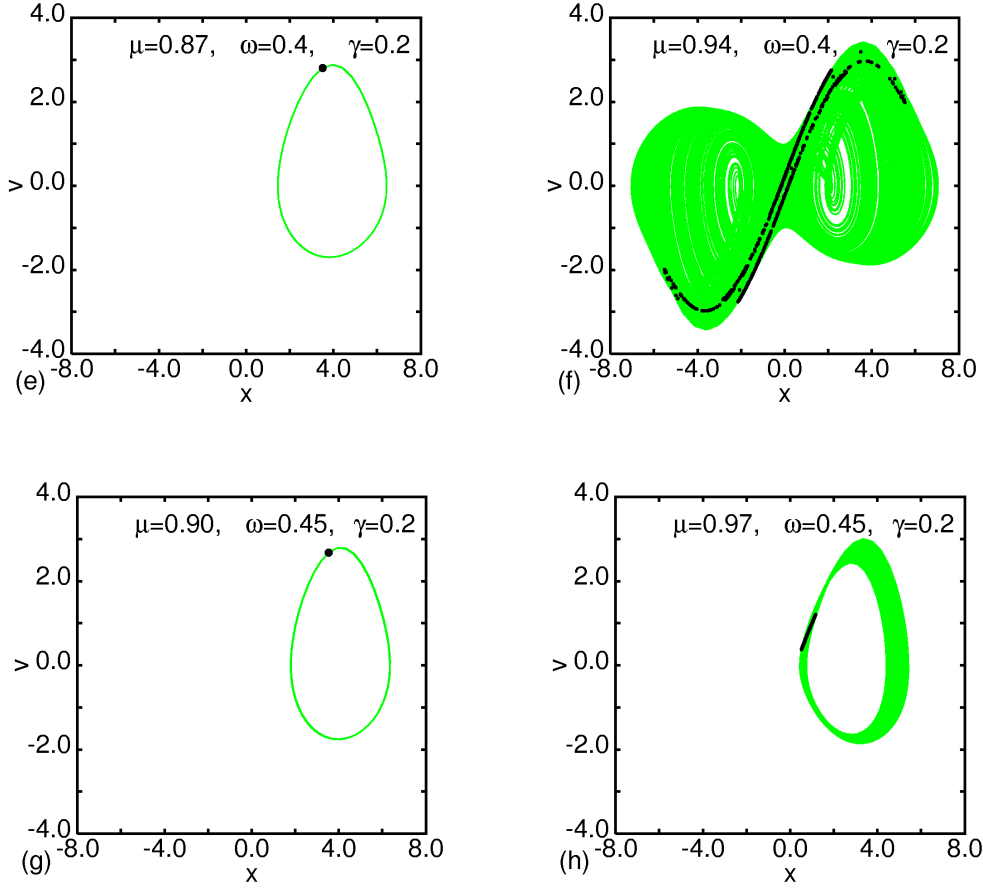


Fig. 5. Continuation.

where the component integrals $I_1(t_0)$ and I_2 are defined:

$$I_1(t_0) = \int_{-\infty}^{\infty} v^*(t)x^*(t) \cos(2\omega(t + t_0))dt \quad (16)$$

and

$$I_2 = \int_{-\infty}^{\infty} (1 - x^{*2}(t)) v^{*2}(t)dt. \quad (17)$$

After evaluation of the above integrals (see Appendix B: Eqs. B.17 and B.4) we get the exact forms of $I_1(t_0)$, and I_2 :

$$I_1(t_0) = \frac{12\pi\delta^2\omega^2(1+4\omega^2)}{\gamma^2 \sinh(2\omega\pi)} \sin(2\omega t_0) \quad (18)$$

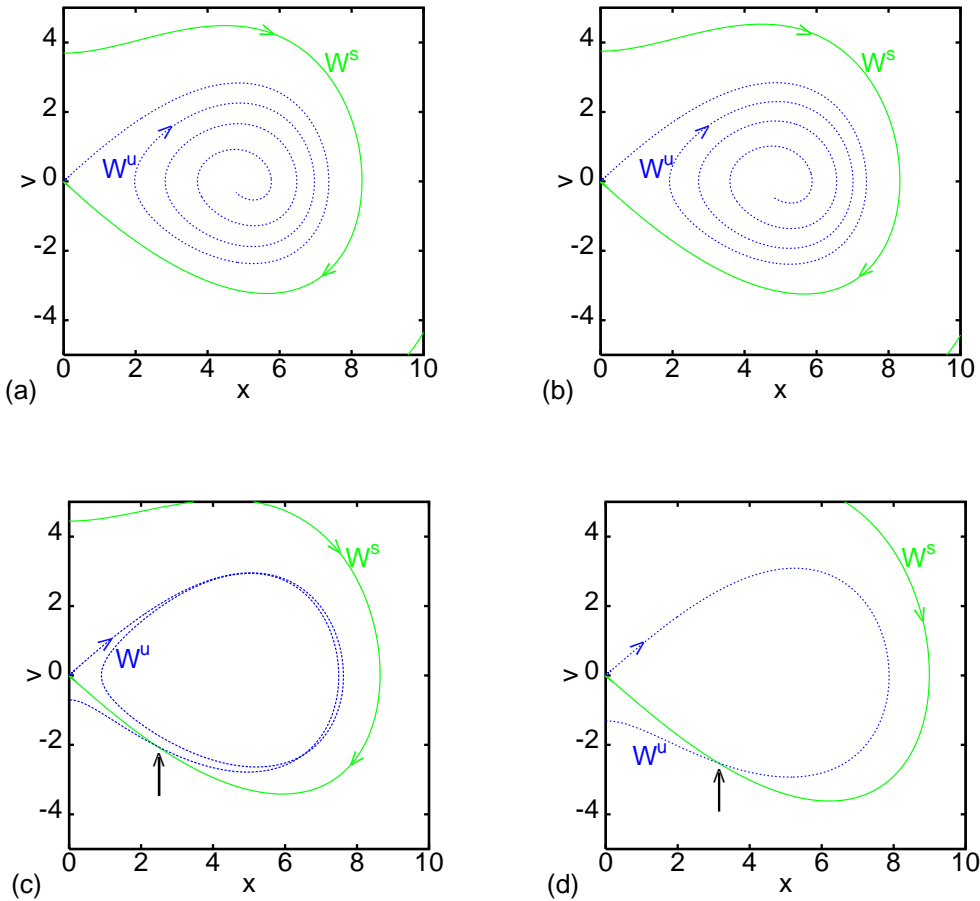


Fig. 6. Stable and unstable manifolds in presence of a perturbation component ($\varepsilon = 0.05$). Parameters used in calculations (Eq. 2): $\omega = 0.4$, $\gamma = 0.2$, $\delta = -1.0$, $\tilde{\alpha} = 0.1$ and various excitation amplitude $\tilde{\mu} = 0.87$ (Fig. 6a), 0.94 (Fig. 6b), 1.8 (Fig. 6c), 2.7 (Fig. 6d). Note that $\mu = \varepsilon\tilde{\mu}$, $\alpha = \varepsilon\tilde{\alpha}$ (see Eq. 3). Arrows in Fig. 6c and d indicate the crossing points.

$$I_2 = \frac{\delta^2 \sqrt{-\delta}}{\gamma^2} \left(-\frac{6}{5} + \frac{72\delta^2}{70\gamma^2} \right). \quad (19)$$

Surprisingly the other choice of system variables (x, w) lead to the same form of Melnikov function (Appendix A), Eqs. 14-17. That means that both perturbation procedures give the same result in the first approximation. This is partially due to the fact that in both cases we started from the same set of equations of unperturbed Hamiltonian H^0 (Eqs. 2,6).

Finally, the condition for a transition to chaotic motion as a global homoclinic transition corresponding to a horse-shoe type of stable and unstable manifolds

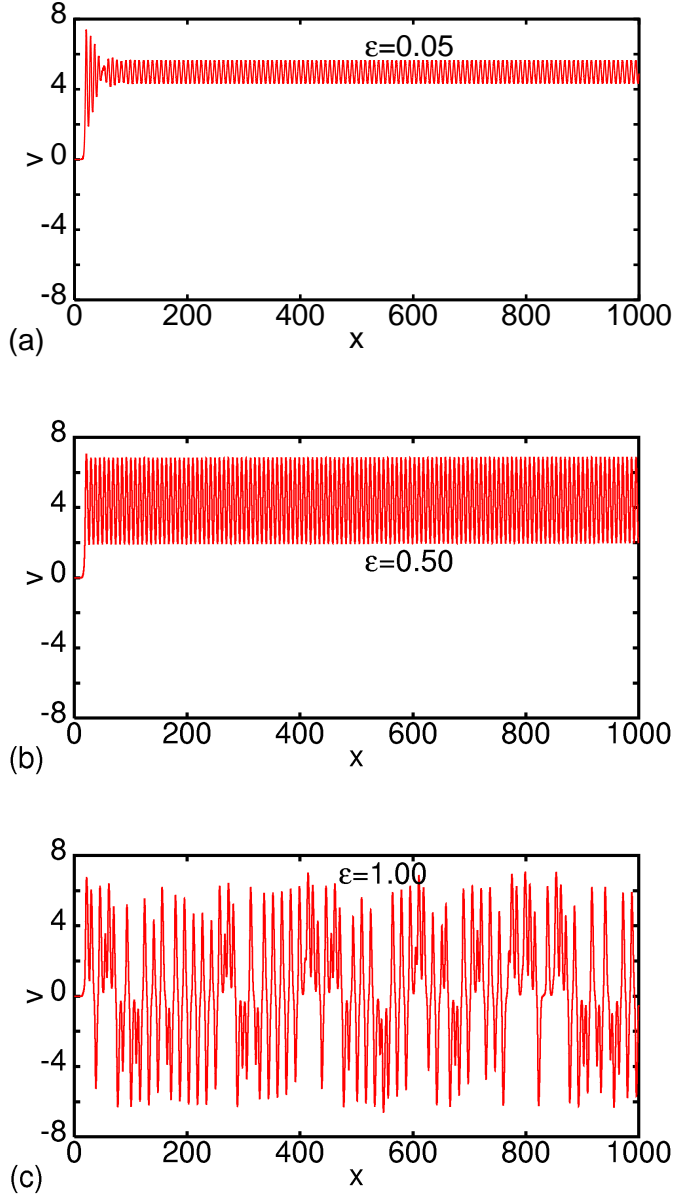


Fig. 7. Time histories $x(t)$ obtained by simulation of Eq. 2 $\omega = 0.4$, $\gamma = 0.2$, $\delta = -1.0$, $\tilde{\alpha} = 0.1$, $\tilde{\mu} = 0.94$ and three values of $\epsilon = 0.05$ (Fig. 7a), $\epsilon = 0.50$ (Fig. 7b), $\epsilon = 1.00$ (Fig. 7c). Note that $\mu = \epsilon\tilde{\mu}$, $\alpha = \epsilon\tilde{\alpha}$ (see Eq. 3).

cross-section, can be written as

$$\bigvee_{t_0} M(t_0) = 0 \quad \text{and} \quad \frac{\partial M(t_0)}{\partial t_0} \neq 0. \quad (20)$$

The above integrals (Eq. 18,19) together with the last condition (Eq. 20) yields

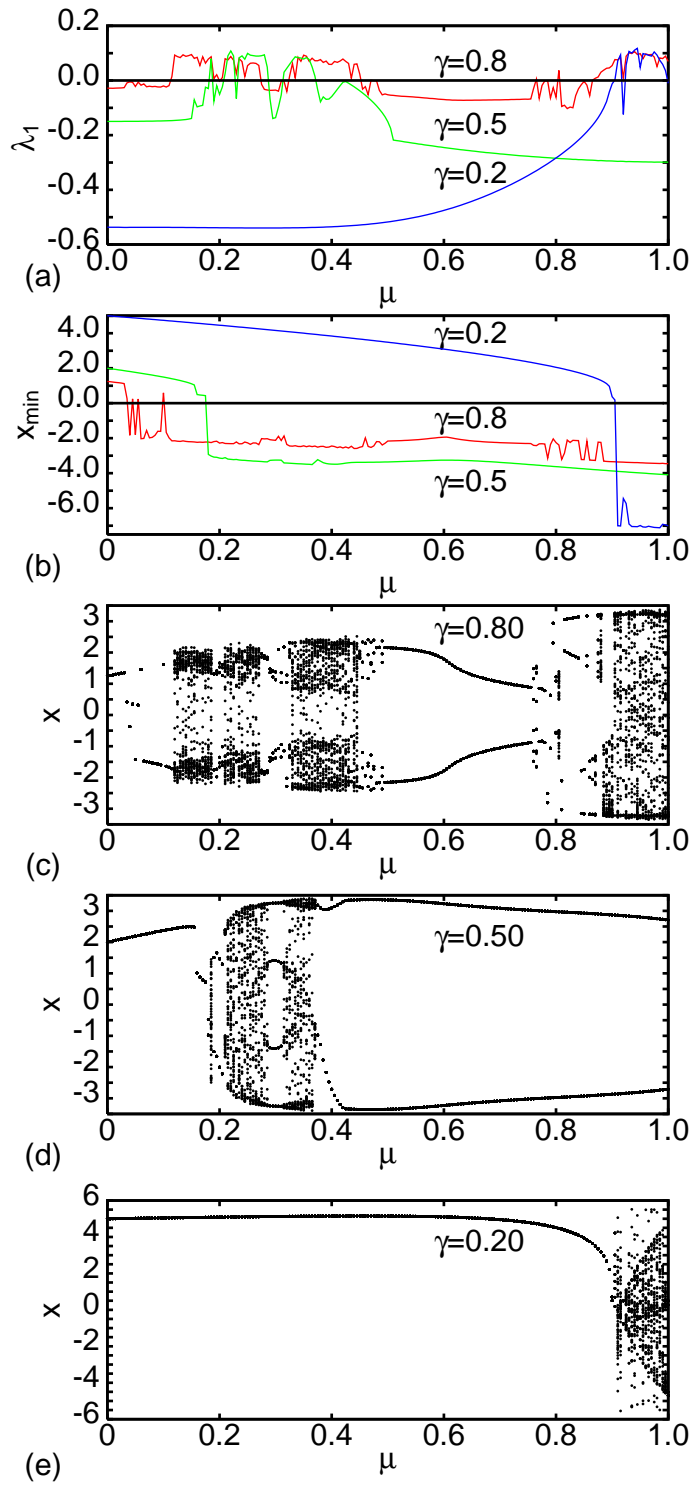


Fig. 8. Maximal Lyapunov exponent λ_1 (Fig. 8a) and the minimum point of displacement point x_{min} (Fig. 8b) of steady state vibrations. Figs. 8d-e correspond to bifurcation diagrams for $\gamma = 0.8, 0.5$ and 0.2 respectively for $\alpha = 0.1, \delta = -1$ and $\omega = 0.4$. Simulations were based on Eq. 1.

a critical value of excitation amplitude μ_c :

$$\mu_c = \frac{\alpha\sqrt{-\delta}\sinh(2\omega\pi)}{12\pi\omega^2(1+4\omega^2)} \left| -\frac{6}{5} + \frac{72\delta^2}{70\gamma^2} \right|. \quad (21)$$

for which stable and unstable manifolds cross.

Namely we get the critical amplitude μ_c versus frequency ω , and parameter γ which is plotted in Figs. 4a–d. Above this value $\mu > \mu_c$ the system transit through a global homoclinic bifurcation which is a necessary condition for appearance of chaotic vibrations. Interestingly, larger γ leads to smaller μ_c (Fig. 4d) Note also, that the condition (Eq. 21) is based on results of perturbation procedure in its lowest order approximation. Equation 21 is the main results of our investigation.

3 Numerical simulations

To verify the analytical findings we have performed series of numerical simulations of Eq. 1. In Fig. 5 we show phase diagrams and simultaneously corresponding Poincare sections stroboscopic points collected with frequency $\Omega = 2\omega$ for chosen sets initial system (Eq. 1) parameters: $\omega = 0.4$, $\gamma = 0.8$ $\mu = 0.02$, 0.10 (Fig. 5a) and $\mu = 0.116$ (Fig. 5b); $\omega = 0.4$, $\gamma = 0.5$ and $\mu = 0.160$ (Fig. 5c) and $\mu = 0.185$ $\omega = 0.4$, $\gamma = 0.2$ (Fig. 5d); $\mu = 0.87$ (Fig. 5e); and $\mu = 0.94$ Fig. 5f); $\omega = 0.45$, $\gamma = 0.2$ and $\mu = 0.90$ (Fig. 5g); and $\mu = 0.97$ Fig. 5h). The structure of the examined attractors as well as calculated Lyapunov exponents enables to classify the dynamics of the system (see Fig. 5 and figure caption). For comparison with analytical results we indicated the simulated cases by points, showing the types of vibrations: R (regular) and C (chaotic). For the last case for relatively small γ ($\gamma = 0.2$ in Fig. 4c, and Figs. 5 e–h) one can see some discrepancy between simulated data and analytical results. Analytical results indicate that the homoclinic transition take place for $\mu_c > 1$ but simultaneously for the same system parameters numerical results states that $\mu_c < 1$ is enough to transit into chaotic vibrations ($\mu_c \approx 1.5$, Fig. 4c). This could be effect of relatively large μ in perturbation procedure (Eq. 3). In the above calculations we used the same initial conditions $(x_{in}, v_{in}) = (0.45, 0.1)$.

The interesting discrepancy between analytical (Fig. 4c) and numerical simulation (Fig. 5e-f) results deserved some additional comments. In this aim we plotted, in Fig. 6) our results on simulations of perturbed system (Eq. 3) related to stable and unstable orbits. Because the Melnikov theory formulated in the lowest order approximation is valid in the limit of small ε ($\varepsilon \rightarrow 0$) we decided to use a relatively small value of this parameter $\varepsilon = 0.05$. Other parameters used in calculations (Eq. 3) are as follows $\omega = 0.4$, $\gamma = 0.2$, $\delta = -1.0$, $\tilde{\alpha} = 0.1$ and various excitation amplitude $\tilde{\mu} = 0.87$ (Fig. 6a), 0.94 (Fig. 6b), 1.8 (Fig. 6c), 2.7 (Fig. 6d). Note, in cases of Fig. 6a and b, which correspond

according to Figs. 4c, 5e, 5f, to regular and chaotic motions for $\varepsilon = 1$ (original equation Eq. 1). Obviously there are no crossing points between the stable W^S and unstable W^U manifolds. After comparing these results it is obvious that in this particular case the final result of our consideration could depend on ε . In fact the difference appears between the limit $\varepsilon \rightarrow 0$ (or $\varepsilon = 0.05$ in Figs. 6a,b) and $\varepsilon = 1.0$, what is not surprise taking into account relatively large value of $\tilde{\mu}$ ($\tilde{\mu} \approx 1.0$ Fig. 4c). Interestingly for the present value of ε ($\varepsilon = 0.05$) our simulations (Fig. 6c and d) confirm analytical predictions (see the solid curve in Fig. 4c). As $\mu > \mu_c \approx 1.5$ in both cases we observe crossing points of the stable and unstable orbits (indicated by arrows in Fig. c and d). Evidently increasing $\tilde{\mu}$ causes faster meeting of corresponding curves W^S and W^U , as one can see Fig. 6c and Fig. 6d differ by winding numbers N of motion necessary for such crossing: $N = 1$ for Fig. 6c and $N = 2$ for Fig. 6d. We have also done additional tests for other system parameters including different $\gamma = 0.5, 0.8$ (as in Fig. 4a-b and Figs. 5a-d) and $\omega = 0.45$ (as in Fig. 4c and Figs. 5g-h). In all cases we have also got agreement with the corresponding analytical curves (Fig. 4). In the next figures (Fig. 7a-c) we show the evolution of the oscillation with increasing ε . Here we have plotted time histories for different values of ε . Starting from vicinity of the saddle point we obtained regular history (Fig. 7a) for $\varepsilon = 0.05$. For larger value of control parameter ε ($\varepsilon = 0.5$ in Fig. 7b) we observe enlargement of the amplitude of these motion and finally its transition to chaotic motion for a large enough ε ($\varepsilon = 1.0$ in Fig. 7c).

For better clarity we decided to show the transition to chaos through the maximal Lyapunov exponent λ_1 and bifurcation diagrams for three values of γ ($\gamma = 0.2, 0.5, 0.8$) versus μ (Fig. 8). Positive value of λ_1 in Fig. 8a(see the region $\sim 0.15 < \mu < \sim 0.45$ for $\gamma = 0.8$) as well as black regions in corresponding bifurcation diagrams (Fig. 8c-e) imply transition to chaos. This is a way of numerical identification of critical value μ_c regarding a local bifurcation. In case of $\gamma = 0.8$ and 0.5 we observe the confirmation of previous findings for numerical (Poincare maps Figs. 5a-d) and analytical results (Fig. 4a-b) while the case of $\gamma = 0.2$ is different. Here again we observe some disagreement between numerical (Figs. 5e-h) and analytical results (Fig. 4c). Lyapunov exponent method gives smaller value of μ_c . The results, obtained while simulating Eq. 1, show the actual critical values of μ for transition to chaotic vibrations. Note also, that in many cases the observe the chaotic oscillations existing in both potential wells (with positive and negative x). However this behaviour is not a rule because Figs. 5g,d show the transition to chaotic behaviour inside the single well $x > 0$. To explore this effect more systematically we plot (in Fig. 8b) x_{min} versus μ and three values of $\gamma = 0.2, 0.5, 0.8$. It appeared that for $\gamma = 0.8$ escapes and returns of the considered system to a single well oscillatory motion can happen for an interval of μ parameter which is close but slightly below the value transition to chaotic vibration. This means that the system has already possessed double well attractor just before its transition to chaotic

behaviour. Note, in our numerical calculations, to have some direct insight into the system capability of transition to chaotic vibration and its escape from the a single well and to minimize the time of our calculations, the initial conditions at the beginning ($\mu = 0$) were assumed to be $(x_{in}, v_{in}) = (0.45, 0.1)$ and continuing the calculations we used final displacement and velocity obtained for the former value of μ (x_{fi}, v_{fi}) as initial conditions for any new value of μ . We also note, that this system resembles the other examined by Thompson [13] with the same type of nonlinearity of square type but without Van der Pol term and external forcing instead of our parametric one. In his study he has got the condition for a global homoclinic transition just before the escape from the single potential well. In our case the effect of self excitation, connected with the Van der Pol damping term is stronger for $\gamma = 0.8$ (Fig. 1). This effect can be deduced from the excitation term itself for $x \rightarrow 0$ we have $VdP(x, \dot{x}) \rightarrow -\alpha\dot{x}$ which means negative damping if the system moves close to $x = 0$. The extra energy generated by such a negative damping makes it possible to overcome the potential barrier between two symmetric potential wells much easier comparing the case without self excitation effect. On the other hand, the size of attractor for given γ (Fig. 5) is solely determined by the shape of the nonlinear potential (Eq. 2, Fig. 1). For $\gamma = 0.8$ we have also found that for $\mu > \mu_c$ a transition chaotic vibrations was preceded by transient chaotic behaviour. The steady state motion undergo escape from a potential well with formation of symmetric attractor spreading on two potential wells. With increasing μ the symmetry of attractor was broken and the system transit a series of period doubling bifurcations as was discussed in earlier papers [7,8,26].

4 Summary and Conclusions

In summary we have studied conditions of a global homoclinic bifurcation in a double well potential –van der Pol system with parametric excitation. Such a bifurcation correspond to transit chaotic behaviour of the system and with some further increasing of the excitation amplitude can lead to the permanent chaos [7,8,14,26].

Using the Melnikov method we have got the analytical formula for transition to chaos in a one degree of freedom, system subjected to parametric excitation with a non-symmetric stiffness with self-excitation term. In our case this effect is mutually introduced through the Van der Pol damping and parametric excitation terms. Our analytical results are consistent with direct computations on homoclinic orbits.

Note that our vector field (Eq. 3) is of C^1 class due to non-continuity of the second derivative at $x = 0$ line or a piece-wise C^2 smooth system. In fact

he standard theory [22] assumes that expansion in Taylor series in ε is good to second order at least (for uniform bounds on ε^2 term). This requires that $h(x, \dot{x})$ and $g(x, \dot{x})$ are of C^2 class with respect to x and \dot{x} , and the Hamiltonian is of C^3 class. However for specific cases the theory can be applied for weaker assumptions. For any non-smooth systems one should check that piece-wise smooth solutions can be assembled and indicate any jumps in derivatives that can occur [25].

Let us write the forms $h(x, \dot{x})$ and $g(x, \dot{x})$ (Eqs. 12 and 13) as vectors:

$$\begin{aligned} \mathbf{h} &= [(\delta x + \gamma |x^*| x^*), v] = [h_1, h_2], \\ \mathbf{g} &= [(\tilde{\mu} x \cos 2\omega\tau + \tilde{\alpha} (1 - x^2) v), 0]. \end{aligned} \quad (22)$$

Now, the Melnikov function $M(t_0)$ can be treated as a projection of the vector $\mathbf{h}^\perp = [-h_2, h_1]$ into the \mathbf{g} direction (a scalar product), Namely

$$M(t_0) = \int_{-\infty}^{\infty} \mathbf{g}(t) \cdot \mathbf{h}^\perp(t + t_0) dt. \quad (23)$$

Note that the vector element h_2^\perp ($h_2^\perp = h_1$) is projected out the Melnikov integral. Moreover the same argument applies to any x derivative of h_1 making its non-smooth behaviour at $x = 0$ unimportant for the Melnikov theory application. In other words this non-smoothness at $x = 0$ is not likely to produce any jump to the homoclinic orbit (Fig. 3).

Interestingly the families of function $\mu_c(\omega)$ plotted against ω scales as $\sim \gamma^{-2}$ leading to small μ_c for relatively large γ ($\gamma = 0.8$) and much larger μ_c for $\gamma = 0.2$. To confirm these results we have performed numerical simulations showing corresponding phase diagrams, Poincare maps Lyapunov exponents and bifurcation maps. The Lyapunov exponent has been calculated using the algorithm provided by Wolf *et al.* [27].

We have noticed some discrepancy (due to relatively large values of μ_c : $|\mu_c/\delta| > 1$), between simulated data and analytical results, especially, in case of small γ . It seems that our Melnikov analysis provides results which are correct up to the first order. The results can be possibly improved in higher order approximations [28] The other possibility is the stronger influence of the Van der Pol term on the system dynamics. However, keeping the Van der Pol term unchanged, we have not analyzed this effect so deep as it deserves leaving this aspect to future studies.

Acknowledgements

This paper has been partially supported by the Polish Ministry of Science and Informatization. GL would like to thank the Max Planck Institute for the Physics of Complex Systems for hospitality. Authors would like to thank Prof. P. Holmes for discussion and unknown reviewers for valuable comments.

Appendix A

The starting equation of motion (Eq. 1) is given as a differential equation of the first order. To perform further analysis of the system it must be split into two equations of the second order. The usual way based on time derivatives of displacement and velocity (x, v) was discussed in Sec. 2 (Eq. 2). The other concept (Eq. 3), connected to division on 'slow' and 'fast' variables leads to a another pair of equations:

$$\begin{aligned} \dot{x} &= w - \varepsilon\tilde{\alpha} \left(x - \frac{x^3}{3} \right) \\ \dot{w} &= -\delta x - \gamma|x|x + \varepsilon\tilde{\mu} (\cos(2\omega t)). \end{aligned} \quad (\text{A.1})$$

The above splitting does not effect the unperturbed Hamiltonian H^0 which is of the same form as for (Eq. 2) Thus w has the same meaning of v but perturbations are now appearing in both equations instead of one.

Now, the gradient of unperturbed Hamiltonian:

$$h = (\delta x + \gamma|x^*|x^*) dx + v dv, \quad (\text{A.2})$$

while g' is a perturbation form

$$g' = (\tilde{\mu}x \cos 2\omega\tau +) dx - \tilde{\alpha} \left(x - \frac{x^3}{3} \right) dv. \quad (\text{A.3})$$

defined on corresponding stable or unstable manifolds $(x, v) = (x^*, v^*)$ (Eq. 10, Fig. 2). The Melnikov function:

$$\begin{aligned} M'(t_0) &= \int_{-\infty}^{+\infty} h(x^*, v^*) \wedge g'(x^*, v^*) dt \\ &= \int_{-\infty}^{+\infty} \left(\tilde{\mu}x^*v^* \cos(2\omega(t+t_0)) + \tilde{\alpha} (\delta x^* + \gamma x^{*2}) \left(x^* - \frac{x^{*3}}{3} \right) \right) dt \end{aligned} \quad (\text{A.4})$$

can be evaluated after substituting $x^*(t)$ and $v^*(t)$ by formulae given in Eq. 10:

$$M'(t_0) = \tilde{\mu}I'_1(t_0) + \tilde{\alpha}I'_2, \quad (\text{A.5})$$

where

$$I'_1(t_0) = \int_{-\infty}^{\infty} dt v^*(t)x^*(t) \cos(2\omega(t + t_0)) \quad (\text{A.6})$$

and

$$I'_2 = \int_{-\infty}^{\infty} dt \left(\delta x^*(t) + \gamma x^{*2}(t) \right) \left(x^*(t) - \frac{x^{*3}(t)}{3} \right). \quad (\text{A.7})$$

Note the expression for $I'_1(t_0)$ (Eq. A.6) coincides exactly with $I_1(t_0)$ analyzed in Sec. 2 (Eq. 16) while I'_2 can be transformed exactly to I_2 if one make use of the definition of the homoclinic orbit parametrisation (Eqs. 7-8) and substituting:

$$\frac{dv}{dt} = -\delta x - \gamma|x|x \quad (\text{A.8})$$

into the expression Eq. A.7 and integrating it by parts:

$$I'_2 = - \int_{-\infty}^{\infty} dt \frac{dv}{dt} \left(x^*(t) - \frac{x^{*3}(t)}{3} \right), \quad (\text{A.9})$$

$$= \int_{-\infty}^{\infty} dt (1 - x^{*2}(t)) v^{*2}(t) = I_2. \quad (\text{A.10})$$

Thus the above Melnikov function form $M'(t_0)$ coincides exactly the the form of $M(t_0)$ obtained Sec. 2 (Eqs. 14–19).

Appendix B

Evaluation of the integral I_2 is straightforward. After substitution $x^*(t)$, and $v^*(t)$ (Eq. 10) we have:

$$I_2 = \int_{-\infty}^{\infty} (1 - x^{*2}(t)) v^{*2}(t) dt \quad (\text{B.1})$$

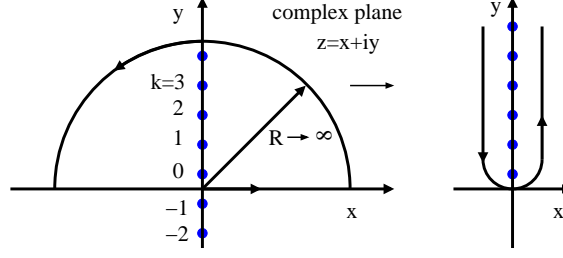


Fig. B.1. Deformed contour integration schema and imaginary poles.

$$= \frac{9 \delta^3}{4 \gamma^2} \int_{-\infty}^{\infty} \frac{\tanh^2 \left(\frac{\sqrt{-\delta t}}{2} \right)}{\cosh^4 \left(\frac{\sqrt{-\delta t}}{2} \right)} \left(1 - \frac{9 \delta^2}{4 \gamma^2} \left(\tanh^2 \left(\frac{\sqrt{-\delta t}}{2} \right) - 1 \right)^2 \right) dt.$$

and simple algebraic manipulations:

$$t = \frac{2\tau}{\sqrt{-\delta}}, \quad \tanh \tau = \xi \quad (\text{B.2})$$

we obtain

$$I_2 = -\frac{9 \delta^2 \sqrt{-\delta}}{2 \gamma^2} \int_{-\infty}^{\infty} \xi^2 (1 - \xi^2) \left(1 - \frac{9 \delta^2}{4 \gamma^2} (\xi^2 - 1)^2 \right) d\xi. \quad (\text{B.3})$$

Finally the result of integration one has a following expression:

$$I_2 = \frac{\delta^2 \sqrt{-\delta}}{\gamma^2} \left(-\frac{6}{5} + \frac{72\delta^2}{70\gamma^2} \right). \quad (\text{B.4})$$

On the the hand the integral I_1 can be written as follows

$$\begin{aligned} I_1(t_0) &= \int_{-\infty}^{\infty} v^*(t)x^*(t) \cos(2\omega(t + t_0))dt \\ &= -\frac{9 \delta^2}{2\gamma^2} \int_{-\infty}^{\infty} \frac{t \sqrt{-\delta}}{2} \frac{\tanh \left(\frac{\sqrt{-\delta t}}{2} \right)}{\cosh^2 \left(\frac{\sqrt{-\delta t}}{2} \right)} \left[1 - \tanh^2 \left(\frac{\sqrt{-\delta t}}{2} \right) \right] \cos(2\omega(t + t_0))dt. \end{aligned} \quad (\text{B.5})$$

what can be expressed further in terms of more elementary integrals I_1^A and I_1^B

$$I_1(t_0) = -\frac{3\delta^2}{2\gamma^2} (I_1^A - 3I_1^B) \sin(2\omega t_0), \quad (\text{B.6})$$

which are given by:

$$I_1^A = \int_{-\infty}^{\infty} \frac{\tanh \tau}{\cosh^2 \tau} \sin \left(\frac{4\omega\tau}{\sqrt{-\delta}} \right) d\tau \quad (\text{B.7})$$

$$I_1^B = \int_{-\infty}^{\infty} \frac{\tanh^3 \tau}{\cosh^2 \tau} \sin \left(\frac{4\omega\tau}{\sqrt{-\delta}} \right) d\tau. \quad (\text{B.8})$$

Note that the second integral I_1^B can be easily obtained from the first one I_1^A through integration by parts

$$I_1^B = \frac{\omega'^2}{12} \left(\frac{8}{\omega'^2} - 1 \right) I_1^A, \quad (\text{B.9})$$

where

$$\omega' = \frac{4\omega}{\sqrt{-\delta}} \quad (\text{B.10})$$

While I_1^A should be calculated using the residue theorem

$$\oint f(z) dz = 2\pi i \sum_{k=1}^N \text{Res}[f(z), z_k], \quad (\text{B.11})$$

where

$$\text{Res}[f(z), z_k] = \frac{1}{(m-1)!} \lim_{z \rightarrow z_k} \frac{d^{m-1}}{dz^{m-1}} [(z - z_k)^m f(z)]. \quad (\text{B.12})$$

In our case

$$f(z) = 4 \frac{\exp(z) - \exp(-z)}{(\exp(z) + \exp(-z))^3} \exp \frac{i4\omega z}{\sqrt{-\delta}} \quad (\text{B.13})$$

where on the real axis (Fig. B.1) $\text{Re} z = \tau$:

$$\text{Im} f(z) = \frac{\tanh \tau}{\cosh^2 \tau} \sin \left(\frac{4\omega\tau}{\sqrt{-\delta}} \right). \quad (\text{B.14})$$

The multiplicity of each pole of the complex function $f(z)$ (Eq. B.13):

$$z_k = \left(\frac{\pi}{2} + \pi k \right) i \quad \text{for } k = 1, 2, 3, \dots \quad (\text{B.15})$$

can be easily determined as $m = 3$. After summation of all poles (Fig. B.1) we get:

$$I_1^A = \frac{8\pi\omega^2}{\delta} \frac{\sin\left(\frac{4\omega z_0}{\sqrt{-\delta}}\right)}{\sinh\left(\frac{2\omega\pi}{\sqrt{-\delta}}\right)}. \quad (\text{B.16})$$

The result of the above analysis can be written in a compact way:

$$I_1(t_0) = \frac{12\pi\delta^2}{\gamma^2} \frac{\omega^2(1+4\omega^2)}{\sinh(2\omega\pi)} \sin(2\omega t_0). \quad (\text{B.17})$$

References

- [1] K. Szabelski, W. Samodulski, Drgania układu z niesymetryczną charakterystyką sztywności przy parametrycznych i zewnętrznym wymuszeniu, *Mechanika Teoretyczna i Stosowana* 23 (1985) 223–238.
- [2] K. Szabelski, The vibrations of self-excited system with parametric excitation and non-symmetric elasticity characteristic, *Journal of Theoretical and Applied Mechanics* 29 (1991) 57–81.
- [3] G. Litak, J. Warmiński, K. Szabelski, Regular and chaotic vibrations of a self-excited system with parametric excitation and non-symmetric elasticity, Proceedings of IUTAM/IFTToMM Symposium on *SYNTHESIS OF NONLINEAR DYNAMICAL SYSTEMS*, 24-28 August 1998, Riga, Latvia (Riga Technical University Eds. E. Lavendelis and M. Zakrzhevsky), 24-28 August 1998, pp. 50–51.
- [4] R.H. Rand, *Lecture Notes on Nonlinear Vibrations* Ithaca: The Internet-First University Press 2003. <http://www.tam.cornell.edu/randdocs/>.
- [5] R. Rusinek, J. Warmiński, Vibrations of Rayleigh-Mathieu oscillator with quadratic elasticity characteristic. *Folia Societatis Scientiarum Lublinensis* 9 (2000) 142–151.
- [6] G. Rega, A. Salvatori, F. Benedettini, Numerical and geometrical analysis of bifurcation and chaos for an asymmetric elastic nonlinear oscillator, *Nonlinear Mechanics* 7 (1995) 249–272.
- [7] W. Szemplińska-Stupnicka, J. Rudowski, Bifurcations phenomena in a nonlinear oscillator: approximate analytical studies versus computer simulation results, *Physica D* 66 (1993) 368–380.
- [8] W. Szemplińska-Stupnicka, The analytical predictive criteria for chaos and escape in nonlinear oscillators: A survey, *Nonlinear Dynamics* 7 (1995) 129–147.

- [9] S. Lenci, G. Rega, Optimal control of homoclinic bifurcation: theoretical treatment and practical reduction of safe basin erosion in the Helmholtz oscillator, *J. Vibr. Control* 9 (2003) 281–315.
- [10] S. Lenci, G. Rega, A unified control framework of non-regular dynamics of mechanical oscillators, *J. Sound Vibr.* 278 (2004) 1051–1080.
- [11] R. Tchoukuegno, B.R. Nana Nbandjo, P. Wofo, Linear feedback and parametric controls of vibrations and chaotic escape in a Φ^6 potential, *Int. J. Non-Linear Mechanics* 38 (2003) 531–541.
- [12] H. Cao, G. Chen, Global and local control of homoclinic and heteroclinic bifurcations, *Int. J. Bifurcation and Chaos* 15 (2005) 2411–2432.
- [13] J.M.T. Thompson, Chaotic Phenomenon Triggering the Escape from a Potential Well, *Proc. Roy. Soc. London A* 421 (1989) 195–225.
- [14] T. Kapitaniak, *Chaotic Oscillations in Mechanical Systems*, Manchester University Press, Manchester 1991.
- [15] J. Warmański, G. Litak, J. Lipski, M. Wiercigroch and M.P. Cartmell, Vibrations in Regenerative Cutting Process, in Synthesis of Nonlinear Dynamical Systems, Eds. E. Lavendelis and M. Zakrzhevsky, SOLID MECHANICS AND ITS APPLICATIONS Vol. 73 (Kluwer Academic Publisher 2000) pp. 275–283.
- [16] S. Li, S. Yang, W Guo, Investigation on chaotic motion in hysteretic nonlinear suspension system with multi-frequency excitations, *Mechanics Research Communications* 31 (2004) 229–236.
- [17] M. Siewe Siewe, F.M. Moukam Kakmeme, C. Tchawoua, Resonant oscillation and homoclinic bifurcation in a Φ^6 -Van der Pol oscillator, *Chaos, Solitons & Fractals* 21 (2004) 841–853. 841–853.
- [18] M. Siewe Siewe, F.M. Moukam Kakmeme, C. Tchawoua, P. Wofo, Bifurcations and chaos in a triple-well Φ^6 -Van der Pol oscillator driven by external and parametric excitation, *Physica A* 357 (2005) 383–396.
- [19] G. Litak, G. Spuz-Szpos, K. Szabelski, J. Warmański, Vibration analysis of self-excited system with parametric forcing and nonlinear stiffness, *Int. J. Bifurcation and Chaos* 9 (1999) 493–504.
- [20] J.L. Trueba, J. Rams, M.A.F. Sanjuan, Analytical estimates of the effect of nonlinear damping in some nonlinear oscillators *Int. J. Bifurcation and Chaos* 10 (2000) 2257–2267.
- [21] J. Awrejcewicz, M.M. Holicke, Melnikov’s method and stick-slip chaotic oscillations in very weakly forced mechanical systems, *Int. J. Bifurcation and Chaos* 9 (1999) 505–518.
- [22] J. Guckenheimer, P. Holmes, *Nonlinear Oscillations, Dynamical Systems and Bifurcations of Vectorfields*, Springer, New York 1983.

- [23] S. Wiggins, *Introduction to Applied Nonlinear Dynamical Systems and Chaos*, Springer, New York 1990.
- [24] S.H. Strogatz, *Nonlinear Dynamics and Chaos*, Perseus Books, Cambridge 1994, p. 212.
- [25] P. Holmes, unpublished, private communication.
- [26] E. Tyrkiel, On the role of chaotic saddles in generating chaotic dynamics in nonlinear driven oscillators, *Int. J. Bifurcation and Chaos* 15 (2005) 1215–1238.
- [27] A. Wolf, J.B. Swift, H.L. Swinney, J.A. Vastano, Determining Lyapunov exponents from a time-series, *Physica D* 16 (1985) 285–317.
- [28] S. Lenci, G. Rega, Higher-order Melnikov functions for single-DOF mechanical oscillators: Theoretical treatment and applications, *Mathematical Problems in Engineering* (2004) 145–168.